2009 IEEE International Conference on Robotics and Automation
Kobe International Conference Center
Kobe, Japan, May 12-17, 2009

Controlling a Robotically Steered Needle in the Presence of Torsional Friction

Kyle B. Reed Allison M. Okamura Noah J. Cowan

Abstract— **A flexible needle can be accurately steered by robotically controlling the orientation of the bevel tip as the needle is inserted into tissue. Here, we demonstrate the significant effect of friction between the long, flexible needle shaft and the tissue, which can cause a significant discrepancy between the orientation of the needle tip and the orientation of the base where the needle is controlled. Our experiments show that several common phantom tissues used in needle steering experiments impart substantial frictional forces to the needle shaft, resulting in a lag of over 45° for a 10 cm insertion depth in some phantoms; clinical studies have reported torques large enough to could cause similar errors during needle insertions. Such angle discrepancies will result in poor performance or failure of path planners and image-guided controllers, since the needles used in percutaneous procedures are too small for state-of-the-art imaging to accurately measure the tip angle. To compensate for the angle discrepancy, we develop a model for the rotational dynamics of a needle being continuously inserted into tissue and show how a PD controller is sufficient to compensate for the rotational dynamics.**

I. Introduction

For many needle-based diagnostic and therapeutic procedures, such as biopsies and prostate brachytherapy, accurate needle tip placement is essential [1], [2]. Guiding a maneuverable needle in real time under image guidance can improve placement accuracy, enable access to multiple targets during a single insertion, and expand the scope of needle interventions by providing the ability to avoid obstacles and reach previously inaccessible subsurface targets.

One mechanism for steering needles involves harnessing the asymmetric reaction forces imparted by tissue on a bevel-tip needle as it is inserted into the tissue. For sufficiently flexible needles, these forces cause the needle to follow a nearly circular arc of constant curvature [3]. The instantaneous direction of curvature can be controlled by rotating the needle about its shaft at the base of the needle (outside the tissue), thereby reorienting the needle tip. The needle tip can then be guided to a desired location inside the body while avoiding obstacles. See [4] for a survey that includes robotically steered needles and insertion modeling.

When rotating the needle inside tissue, friction between the tissue and the inserted length of the needle results in the angle of the needle tip "lagging" the angle of the needle base. We show that several tissue phantoms impart sufficient frictional forces to the needle shaft to cause significant discrepancies between the base and tip angles. Podder et al. [5] found torques large enough to cause the needle in human tissues to similarly twist during clinical needle insertions for prostate brachytherapy.

When steering a needle using an asymmetric tip, any inconsistency between base and tip orientations or misalignment of the needle tip can result in poor performance or failure of controllers and path planners. Reed et al. [6] demonstrated that using a pre-bent needle tip instead of a bevel-tip needle caused deviations in the tip location when the needle was rotated. The small discrepancy caused the robotically controlled needle to puncture the obstacles and miss the targets.

Current medical imaging technology does not enable direct measurement of the bevel angle around the needle shaft due to the small diameter of the needles used in clinical procedures. Ultrasound and other imaging techniques can achieve a resolution of 0.8 mm [7], which is similar to the diameter of needles used in many percutaneous procedures. At these resolutions, imaging alone is unable to determine the roll of the bevel tip. Kallem and Cowan [8] describe an image-based state estimation approach to recover the needle shaft orientation in real time, but their controller assumes that changes in the base angle directly relate to changes in the tip angle. Our torsion controller is designed to work with controllers such as their planar controller to decrease the convergence time.

Several papers [8], [9], [10], [11], [12] mention the possibility that torsional friction along the inserted portion of the needle could be a problem, but the authors are not aware of any work quantifying this effect in multiple tissues or during continuous insertion. Abolhassani et al. [9] and Reed [13] describe a method of adjusting the needle rotation based on the torque measured at the base of the needle while the needle is not moving in translation. Several studies examine the friction required to insert a needle into tissue [14], [15], but not the friction when rotating. This paper demonstrates the severity of torque generated at the needle–tissue interface and formulates a model of the rotational dynamics that can be incorporated into path planners and position estimators for steerable needles [6].

II. Quantifying Needle Tip Lag

A. Materials and Methods

We used the device shown in Figure 1 for our measurements and experimental validation. The setup is capable of rotating and inserting a needle into tissue using two DC servo motors. A 6-axis sensor (ATI Nano 17) measures the forces and torques at the base of the needle.

This work was supported by NIH grant R01 EB006435. K. Reed, A. Okamura, and N. Cowan are with the Department of Mechanical Engineering at The Johns Hopkins University. {reedkb,aokamura,ncowan}@jhu.edu

TABLE I

TISSUE AND PHANTOM DESCRIPTIONS

Material	Description	Vendor
Chicken breast	Needle inserted parallel to muscle fibers	Costco, Inc.
Soft Plastisol	Fabricated using plastic:softener (stock # 2228 LP and 2228 S, respectively) of 32:9	M-F Mfg Co, Inc.
Hard Plastisol	Fabricated as above using plastic:softener of 4:1	M-F Mfg Co, Inc.
Porcine gelatin	Fabricated using a ratio of 5 tbsp (74 cm^3) of powder (part # G2500) to 1 cup (237 cm^3) of water	Sigma-Aldrich Co.
SimTest	Ballistics gel typically used for high velocity impact tests	Corbin, Inc

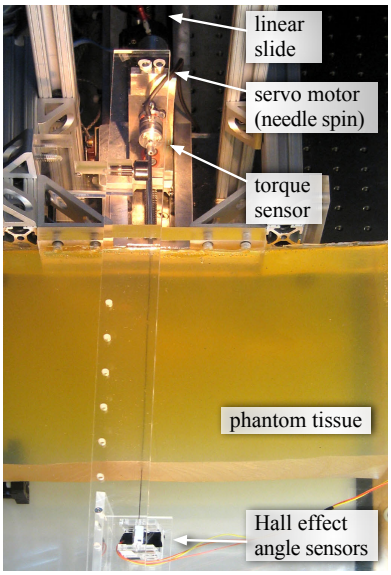

Fig. 1. **Experimental setup:** After inserting, the protruding needle tip was attached to a hall effect angle sensor. The tip and base angles were measured as the needle was stationary and as the needle moved through the tissue. The needle angles and torque exerted at the base were measured in multiple tissues at multiple lengths.

For this experiment, we inserted a solid 0.59 mm diameter nitinol wire (Nitinol Devices and Components, Fremont, CA) through five tissue types (Table I). We inserted the needle in an approximately straight path by rotating the needle 180° every 1 cm. After inserting, we instrumented the protruding needle to measure the angle of the needle tip. Set screws held two magnets on opposite sides of the needle. A hall effect sensor (Honeywell Sensing and Control, Golden Valley, MN, USA) was attached to a platform that translates with the needle base to maintain the proper distance to the magnets. Extending the needle through the tissue eliminates the effect of the bevel tip on rotation, thus isolating the effect of shaft friction.

We performed two types of experiments with rotating needles: 1) the needle was not translating and 2) the needle was translating. In the non-translating experiments, the distance between the needle base and tissue was 23 cm. Each material was tested at an insertion depth of 10 cm and the porcine gelatin was additionally tested at 2.5, 5, and 7.5 cm. One test consisted of rotating the needle base by 90° and the second consisted of rotating the needle base clockwise and counterclockwise by 90°. Both variations ended by retracting the needle 0.5 cm to test the effects of stiction.

For the translating experiment, the needle base started 5 cm from the tissue, as shown in Figure 1, and retracted at a velocity of 0.25 cm/sec. To reduce the effects of the needle buckling inside the support sheath, we retracted the needle instead of inserting. Buckling would cause the needle to press against the sheath and cause a further lag between the tip and the base. Since the tip is not cutting through the tissue, there is minimal difference between retracting and inserting. The plastisol was tested at depths of 5, 10, and 20 cm.

B. Tip Lag without Needle Translation

1) Tissue Effects: Torsional friction is a significant problem for all the phantoms listed in Table I. Figure 2 shows the lag associated with rotating the needle base 90°. The plastisols have a lag of about 10° and show considerable creep once the base has stopped rotating. SimTest gel shows a similar, yet more significant, creep effect during the same time period. Porcine gelatin[1] exhibits the most dramatic "stick-slip" behavior of the tissue samples tested, indicative of substantial stiction; for this material the needle almost immediately reaches steady state when the base rotation halts.

[1]We also tested the same porcine gelatin sample at different temperatures and over several days. The lag and angle profiles for all these tests were similar to those shown here.

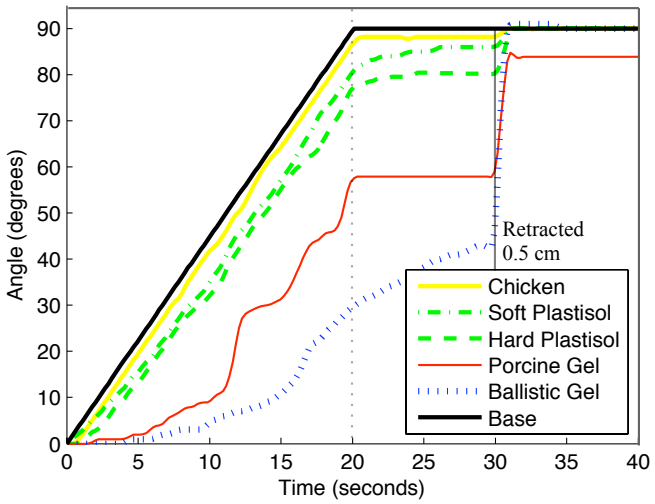

Fig. 2. **Torsion behavior in multiple materials**: For each material, the needle base was rotated 90° over 20 sec, and then held stationary for 10 sec. Each tissue had enough friction to cause significant torsional lag at the tip. At $t = 30$ sec, the needle was retracted 0.5 cm to break the stiction, which caused the needle tip to snap to the correct angle in most materials.

The experimental procedure used here is ideal for plastisols because the needle was rotated slowly. Plastisols exhibit significant damping characteristics, so we suspect that the needle–tissue friction will increase at higher rotational velocities.

The chicken breast showed little torsion lag. Since chicken breast has tissue structures similar to human muscle tissue it may provide comparable results; however, we caution that the chicken was previously frozen and packaged in fluid and may therefore exhibit significantly less friction. Moreover, the chicken model is not necessarily a good predictor of behavior in other human tissue (e.g. prostate [5], fat).

2) Depth Effects: As expected, the depth of insertion affects the torsion lag. Figure 3 shows the lag associated with rotating the needle base at four different depths in porcine gelatin. Torsional friction should be a function of depth since more tissue interacts with the needle at deeper insertions [15].

Figure 3 also shows other complications associated with torsion windup. At $t = 30$ sec, the tip begins to rotate back to $0°$ as the base rotates back. The tip is briefly leading the base. At a depth of 10 cm, the needle tip has rotated by almost $20°$ before the base overtakes the tip. This lead effect is likely due to tissue elasticity; the tissue briefly pulls the needle in the same direction as the base. The tissue, rather than the base actuator, is causing the tip to rotate during this early reversal period.

3) Overcoming Torsional Stiction: The final motion in Figures 2 and 3 is the needle base retracting 0.5 cm. This motion allows the needle to release much of its torsional energy by breaking the stiction at the needle-tissue interface and allows the needle to snap near to the final base angle. The required retraction distance is a function of the elasticity of the tissue; more elastic materials will require a larger retraction.

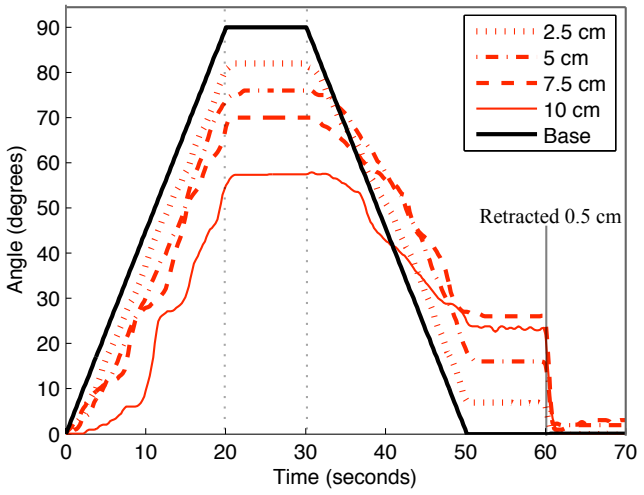

Fig. 3. **Torsion behavior for insertion to multiple depths**: For a single material (porcine gel), the needle tip lag was tested at multiple depths. The base was successively rotated $90°$ clockwise over 20 sec, held stationary for 10 sec, and rotated $90°$ counterclockwise over 20 sec. At $t = 60$ sec, the needle was retracted 0.5 cm. The tip lag increases with increased insertion depth.

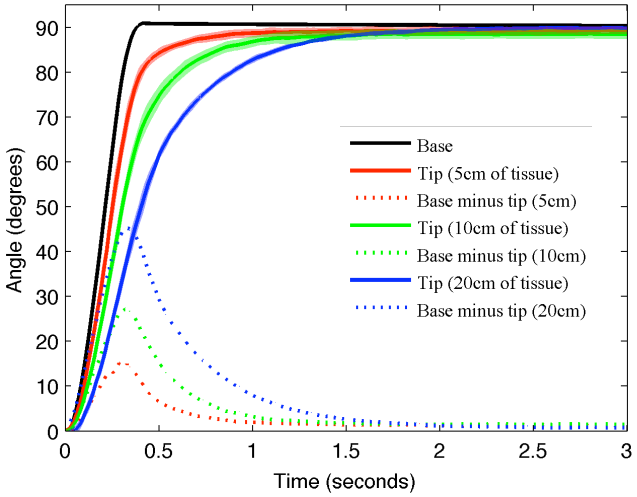

Fig. 4. **Torsion behavior during continuous motion**: For a single material (plastisol), the needle base was quickly rotated $90°$ while the needle was retracted at 0.25 cm/sec through three depths. The tip takes longer to settle to the base angle when inserted through more tissue. There is a significant lag for about two seconds, which can cause errors in the trajectory. Each depth is the average of 10 trials.

One method to overcome the lag is to retract the needle by a small amount after rotating and then reinsert the needle the same distance. Retracting the needle will leave a precut needle path. Upon reinsertion, the needle will likely follow this precut path and return to the previous location with the bevel tip at the desired orientation. Additional forward insertion will cause the needle to follow a new path defined by the new tip angle. This method is not recommended in real tissue since it may cause additional tissue damage. Also, this method will likely fail for a prebent needle since it may follow a different path upon reinsertion.

C. Tip Lag with Needle Translation

Even when the needle is continuously moving through tissue, the tip still lags the base when rotated. Figure 4 shows the lag associated with rotating a needle in 10 cm of soft plastisol while the needle is being retracted at 0.25 cm/sec. Similar to the non-translating case, more tissue contact causes a larger tip lag. Whereas the non-translating case would remain at a constant lag, continuously inserting causes the tip to asymptotically approach the base angle. Table II shows the coefficients for an exponential curve fit for the difference between the tip and base angles once the base has reached $90°$ ($t \approx 0.4$ sec in Figure 4). We will describe the mechanics model used to derive the exponential fit in Section III.

TABLE II

COEFFICIENTS OF TIP LAG DURING CONTINUOUS INSERTION

	$\theta_{\text{lag}} = c_1 \exp\{-c_2 t\}$			damping
depth	c_1	c_2	R^2	b (N-mm-s)
5 cm	12.0	5.0	0.986	0.64
10 cm	25.1	4.1	0.999	0.78
20 cm	42.5	2.7	0.999	1.18

D. Clinical Implications

Podder et al. [5] measured the forces and torques during several prostate brachytherapy needle interventions. Compared to the torque in the other two directions, the torque around the insertion axis appears minuscule, but the 7 N-mm they did measure is actually higher than the torque measured in SimTest gel (1.0 N-mm) when it had a lag of nearly $50°$. Reed [13] shows that the lag at certain instances can be calculated from the torque measured at the base of the needle as

$$\theta_{\text{base}} - \theta_{\text{tip}} = \frac{\tau_{\text{base}}}{JG}\left(\frac{l_{\text{in}} + l_{\text{out}}}{2}\right), \tag{1}$$

where l_{in} and l_{out} are the distances from the base of the needle to the tissue and the tip of the needle, respectively, τ_{base} is the torque measured at the base of the needle, G is the shear modulus of the needle, and J is the polar moment of inertia of the needle.

The 7 N-mm of torque reported by Podder et al. for a human intervention would cause a lag of about $11°$ in a 1.27 mm diameter nitinol needle of the same 20 cm length inserted 5 cm into tissue. Podder et al. used larger stainless steel needles, which will reduce the amount of lag due to increased diameter and stiffness. However, tip-steerable needles require the superelastic properties of materials such as nitinol, so it is likely that torsion windup will be an issue in human tissues.

III. Needle Torsion Model

At certain instances, the torque at the needle base directly relates to the steady state lag at the needle tip as shown in (1), but this equation says nothing about the trajectory of the needle tip. Here, we develop a model of the needle dynamics rotating inside tissue.

When a needle is moving through tissue at a constant speed, the surface of the needle is continuously sliding past the tissue. The experiments in Section II-C show that the needle tip eventually reaches the base angle, which shows that stiction effects are diminished when the needle is moving through tissue. Our model assumes that each part of the needle is moving relative to the local tissue such that the interaction with the tissue can be assumed to be viscous only and the effects of stiction will not be present.

Figure 5 shows our model of the torque exerted on a small element of the needle inside tissue. Writing Newton's Second Law for this small element results in

$$\frac{\partial \tau}{\partial x}dx - D\frac{\partial \theta}{\partial t}dx = \rho_n J \frac{\partial^2 \theta}{\partial t^2}dx, \tag{2}$$

where τ is the torque exerted on this element from neighbor elements (internal torque), x is the distance along the length of the needle, D is viscous damping exerted on an element, t is time, θ is the angle, and ρ_n is the density of the needle.

As shown in Section II-B.2, the total lag increases with insertion depth since additional tissue interacts with the needle. Assuming homogeneous tissue, the total torsional friction should increase linearly since each additional piece

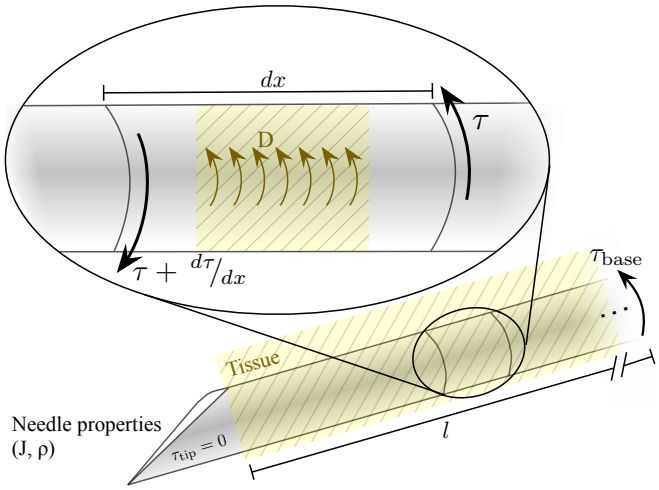

Fig. 5. **Needle model**: The torque from neighboring elements and the damping from the tissue act on each small element of the needle.

of tissue will exert an additional resistive force. Thus we model the friction at each small element as

$$D = \frac{b}{l}, \tag{3}$$

where b is the effective damping coefficient along the entire needle–tissue interface of length l.

Mechanics principles give the torque between two points on a cylinder (the needle in this case) as

$$\theta = \int_0^l \frac{\tau(x)dx}{J(x)G(x)}. \tag{4}$$

The needle has constant material properties, so $J(x) = J$ and $G(x) = G$. Taking the partial derivative of (4) with respect to x results in

$$\frac{\partial \tau}{\partial x} = JG\frac{\partial^2 \theta}{\partial x^2}. \tag{5}$$

Substituting (5) into (2) and integrating results in a homogenous partial differential equation that defines the motion of the needle through time and space.

$$JG\frac{\partial^2 \theta}{\partial x^2} = \rho J \frac{\partial^2 \theta}{\partial t^2} + D\frac{\partial \theta}{\partial t}. \tag{6}$$

To control the orientation of the needle, a torque is exerted at the base. The torque can be represented as a spatial impulse function

$$P(x,t) = \delta(x)u(t), \tag{7}$$

where δ is the Dirac Impulse function and $u(t)$ is the input torque. The forced partial differential equation is

$$\rho J \frac{\partial^2 \theta}{\partial t^2} + D\frac{\partial \theta}{\partial t} - JG\frac{\partial^2 \theta}{\partial x^2} = P(x,t). \tag{8}$$

The ends of the needle can move freely, so the boundary conditions can be expressed as

$$\frac{\partial \theta(0,t)}{\partial x} = 0 \tag{9a}$$

$$\frac{\partial \theta(l,t)}{\partial x} = 0. \tag{9b}$$

We assume the solution is separable in time and space, so we can write

$$\theta(x,t) = \sum_{n=1}^{\infty} \psi_n(x) q_n(t), \tag{10}$$

where $\psi_n(x)$ is the shape function describing the n^{th} mode and $q_n(t)$ is the associated time dependent factor. Using the boundary conditions specified in (9), the general solution for each mode shape is

$$\psi_n(x) = \cos(\omega_n x), \tag{11}$$

where ω_n is the frequency of the n^{th} mode and

$$\omega_n = \frac{n\pi}{l} \quad n = 0, 1, 2, 3, \ldots \tag{12}$$

Plugging (10) into (8) results in

$$\sum_{n=0}^{\infty} \{\rho J \psi_n \ddot{q}_n + D\psi_n \dot{q}_n - JG\omega_n^2 \ddot{\psi}_n q_n\} = P(x,t). \tag{13}$$

Each mode is orthogonal to every other mode, so we can apply the orthogonality principle by multiplying (13) by an arbitrary mode shape (ψ_s) and integrating over the length. The orthogonality principle shows that

$$\int_0^l \psi_n(x)\psi_s(x)dx = 0.5\delta_{ns} \tag{14}$$

and, since $\psi_n(x)$ is a function of cos,

$$\int_0^l \ddot{\psi}_n(x)\psi_s(x)dx = -0.5\delta_{ns} \tag{15}$$

where δ_{ns} is the Kroenecker delta defined as

$$\delta_{ns} = \begin{cases} 0 & n \neq s \\ 1 & n = s \end{cases} \tag{16}$$

and in the 0^{th} mode, $\delta_{00} = 2l$ since $\psi_0(x) = 1$ is constant.

For many types of damping, the modal coordinates cannot be decoupled. However, a proportionally (viscously) damped system has the same mode shapes as the equivalent undamped system, so it can be decoupled by using modal coordinates.

The sifting property of the Dirac function at $x = 0$ shows

$$\int_0^l P(x,t)\psi_s(x)dx = u(t)\int_0^l \delta(x)\psi_s(x)dx = u(t), \tag{17}$$

which means that any input at the base will excite all modes.

The final solution for the n^{th} mode is

$$\rho J \ddot{q}_n(t) + D\dot{q}_n + JG\omega_n^2 q_n(t) = u(t) \tag{18}$$

and can be truncated to any number of uncoupled modes. For the thin needles we used, ρJ is very small compared to b and JG and the system is highly over-damped, so we will use an inertialess model where $\rho J = 0$.

The high frequencies will damp out faster than the low frequencies, so the lowest frequency will have the longest lasting effect on the tip lag. As an approximation to the tip lag, we truncated the model in (18) to a first order model so the angle at the tip is

$$\theta_{\text{base}} - \theta_{\text{tip}} = c \exp\left(-\frac{JG\pi^2}{bl}t\right), \tag{19}$$

where c is a constant depending on initial conditions. In Table II, we calculated the damping based on (19) using the tip rotations shown in Figure 4.

IV. Results

To compare our model and the actual dynamics, we applied a chirp function to the needle base and measured the response at the needle tip, shown in Figure 6. The open loop characteristics show an attenuation as the frequency increases. At frequencies below 2 Hz, there are no oscillatory modes because the effects of damping greatly exceed the low mass and stiffness. At higher frequencies, the rotation motor dynamics became more prevalent because the transmission was not designed for large rapid oscillations. Continuous rapid oscillations are not recommended, since they are likely to cause excessive tissue damage.

We simulated the same chirp function on a first order truncated version of the model shown in (18). Figure 6 shows that the modeled dynamics are similar to the experimental open-loop characteristics. One specific difference is that the open-loop response is consistently at a lower angle than the modeled dynamics. This is likely caused by tissue elasticity. When the needle angle reaches the top peak, the tissue continues to pull in the opposite direction and does not begin opposing motion until the needle has rotated past the equilibrium point in the tissue. The equilibrium point for the needle in the elastic tissue is less than the center of the oscillations. Oscillating the needle amplifies the tissue elasticity effect.

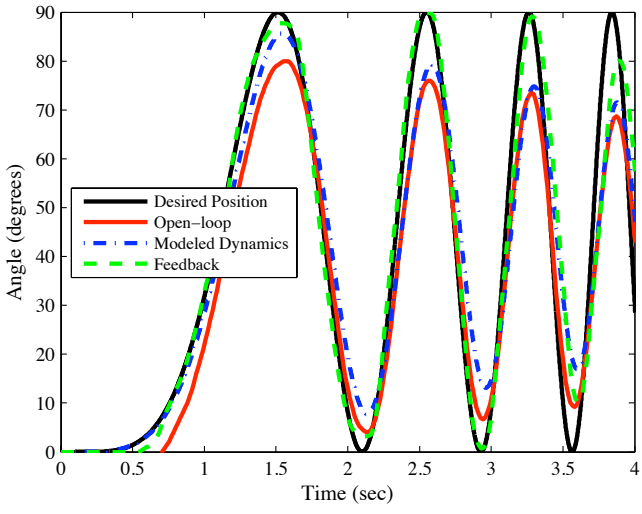

Fig. 6. **Response to chirp function:** While the needle was translating at 0.25 cm/sec through 10 cm of tissue, we applied a sinusoidal chirp function to the needle base at frequencies from 0.1 Hz to 4 Hz. The above plot shows the responses for the open-loop, modeled dynamics, and feedback controlled conditions.

No direct feedback is typically available for feedback control, but our torsion model is designed to work in conjunction with an estimator and the planar controller derived by Kallem and Cowan in [8]. They designed an observer to estimate the needle tip rotation angle and their planar controller controls the needle rotation in order to drive the needle tip to a desired plane using image feedback. When comparing experiments to simulations, they found that the real system converged slower than simulations, which they speculated was due to unmodeled torsion dynamics. For a further understanding of how the tip angle controller integrates with the planar controller, see [6].

To demonstrate that a feedback controller is sufficient, we performed an experiment with PD feedback from the measured needle tip angle. In future work, the measured angle will use an estimate of the tip angle based on the base angle and modeled dynamics. Figure 6 shows the feedback response to the same chirp frequency that we applied to the open-loop and modeled systems. At frequencies less than $1.5\,\mathrm{Hz}$, the feedback controller was able to keep the tip at the desired angle. At higher frequencies, the response began to attenuate, largely due to the limited bandwidth of the rotation motor. Based on these experiments, the torsion model should enable us to enhance Kallem and Cowan's [8] planar controller by incorporating the extra torsion state into their observer–controller pair.

V. Conclusions

Friction is detrimental to accurate control of steerable needles, both in the phantom tissues tested here and likely in human tissues, particularly when using superelastic needles to enhance steering. In our experiments, torsional friction caused a discrepancy of over 45° between the base and tip angles in certain phantom materials. We estimate that in procedures such as prostate brachytherapy it could cause a 10° to 15° discrepancy in tip angle for human tissues based on previous experiments with steel needles [5]. It is possible that torsional forces could be amplified by lateral forces on the needle during insertion into human tissue, which may account for some of the high torques during those needle insertions. Such significant errors will likely imperil image-guided controllers and path planners designed for flexible needle steering. Unfortunately, there is a trade off between a needle that is flexible enough to steer versus a needle that is sufficiently stiff to rotate as a rigid body inside a tissue.

We derived the torsion dynamics for a needle continuously translating through tissue. We demonstrated that a PD controller can compensate for torsion and that our model should integrate well with a controller designed to maintain the needle near a plane. The open loop characteristics closely match our modeled dynamics, so using an estimator in place of the measured angle should allow accurate control of the needle inside tissue.

If a steerable needle is controlled by a robot or a clinician via teleoperation, estimating the torque may be important. Clinicians steering a needle will likely occasionally stop and rotate before further insertion. When they subsequently insert further, the initial inaccuracies following a rotation can cause path deviations. It may be necessary to automatically compensate or provide feedback to the clinician about the torque on the needle. One mode of feedback might be an amplified version of the torsional stiffness. This would be particularly important for pre-bent needles that are not translating into the tissue.

Acknowledgments

The authors thank John Swensen and Tom Wedlick for help with the needle steering device.

References

[1] S. Nath, Z. Chen, N. Yue, S. Trumpore, and R. Peschel, "Dosimetric effects of needle divergence in prostate seed implant using I and Pd radioactive seeds," *Medical Physics*, vol. 27, pp. 1058–1066, May 2000.

[2] J. H. Youk, E. K. Kim, M. J. Kim, J. Y. Lee, and K. K. Oh, "Missed breast cancers at US-guided core needle biopsy: How to reduce them," in *Radiographics*, vol. 27, Jan-Feb 2007, pp. 79–94.

[3] R. J. Webster III, J. S. Kim, N. J. Cowan, G. S. Chirikjian, and A. M. Okamura, "Nonholonomic modeling of needle steering," *The International Journal of Robotics Research*, vol. 25, no. 5-6, pp. 509–525, 2006.

[4] N. Abolhassani, R. Patel, and M. Moallem, "Needle insertion into soft tissue: A survey," *Medical Engineering and Physics*, vol. 29, pp. 413–431, 2007.

[5] T. Podder, D. Clark, J. Sherman, D. Fuller, E. Messing, D. Rubens, J. Strang, L. Liao, W. Ng, and Y. Yu, "In vivo motion and force measurement of surgical needle intervention during prostate brachytherapy," *Medical Physics*, vol. 33, no. 8, pp. 2915–2922, 2006.

[6] K. B. Reed, V. Kallem, R. Alterovitz, K. Goldberg, A. M. Okamura, and N. J. Cowan, "Integrated planning and image-guided control for planar needle-steering," in *Proc. IEEE Conf. Biomedical Robotics*, October 2008, pp. 819–824.

[7] M. Ding and H. Cardinal, "Automatic needle segmentation in three-dimensional ultrasound image using two orthogonal two-dimensional image projections," *Medical Physics*, vol. 30, no. 2, pp. 222–234, 2003.

[8] V. Kallem and N. J. Cowan, "Image guidance of flexible bevel-tip needles," *IEEE Trans. Robotics*, in press.

[9] N. Abolhassani, R. V. Patel, and F. Ayazi, "Minimization of needle deflection in robot-assisted percutaneous therapy," *Int. Journal of Medical Robotics and Computer Assisted Surgery*, vol. 3, pp. 140–148, 2007.

[10] V. Kallem, D. E. Chang, and N. J. Cowan, "Task-induced symmetry and reduction in kinematic systems with application to needle steering," in *IEEE/RSJ Int. Conf. Intelligent Robots and Systems (IROS)*, pp. 3302 – 3308.

[11] R. Alterovitz, A. Lim, K. Goldberg, G. S. Chirikjian, and A. M. Okamura, "Steering flexible needles under markov motion uncertainty," in *IEEE/RSJ Int. Conf. on Intelligent Robots and Systems (IROS)*, 2005, pp. 120–125.

[12] R. J. Webster III, J. Memisevic, and A. M. Okamura, "Design considerations for robotic needle steering," in *IEEE Int. Conf. on Robotics and Automation (ICRA)*, 2005, pp. 3588–3594.

[13] K. B. Reed, "Compensating for torsion windup in steerable needles," in *Proc. IEEE Conf. Biomedical Robotics*, 2008, pp. 936–941.

[14] H. Kataoka, T. Washio, K. Chinzei, K. Mizuhara, C. Simone, and A. M. Okamura, "Measurement of the tip and friction force acting on a needle during penetration," in *Proc. Medical Image Computing and Computer Assisted Intervention (MICCAI)*, 2002, pp. 216–223.

[15] A. M. Okamura, C. Simone, and M. D. O'Leary, "Force modeling for needle insertion into soft tissue," *IEEE Trans. Biomedical Engineering*, vol. 110, no. 51, pp. 1707–1716, 2004.